Improving Structural Integrity with Boron-Based Additives for 3D printed 420 Stainless Steel

Truong Do[*], Chang Seop Shin, Dalton Stetsko, Grayson VanConant, Aleksandr Vartanian, Shenli Pei and Patrick Kwon[2†]

[1]*Michigan State University, East Lansing, MI, U.S.A.*
[*]*dotruong@msu.edu*, [‡]*pkwon@egr.msu.edu*

Abstract

This paper explores the possibility of attaining fully dense parts with a powder-based 3D printing method by sintering, instead of following the standard protocol of infiltrating bronze. The possible ingredients that can be added to improve the densification are explored, which will also enhance the structural integrity of 3D printed 420 stainless steels (SS). As studied with the powder metallurgy (P/M) community in the past half of a century, a small addition of ingredients (sintering aid) into a base metal powder enhances densification and improves the final structural integrity. Numerous P/M works have suggested possible ingredients as sintering aids. However, these P/M works were not carried out with a consistent set of experimental conditions. Thus, in this study, we have constrained our base powder to be 420 SS, common for 3DP, with the average size of 30 micron, which were sintered between 1150 and 1250°C after the powder were mixed with the sintering ingredients. Each sintered sample was analyzed in terms of the final density attained, the amount of ingredient mixed and the sintering temperature.

Keywords: 3D Printing, Sintering Aids, Densification, Homogeneous improvement in properties

1 Introduction

Conners et al. (2014) have defined the three-axis model - Volume, Complexity and Customization – to categorize manufactured products to examine additive manufacturing (AM) on these axes. However, Complexity and Customization axes share many similar traits in manufacturing. It is also noted that the main advantage of AM is in the complexity, both geometric complexity and variation complexity, which enable us to provide customized parts. To understand the relationship between AM and traditional manufacturing processes, we defined slightly different three axes, scale (s), complexity (c) and integrity (i). Here, the scale means both volume (size) and quantity while the complexity means both the complexity as well as the customization. The (structural) integrity axis is added to truly represent the current status of AM. The three axes are presented in Figure 1. In Figure

---

[*] First Author
[†] Corresponding Author
[‡] Corresponding Author

1, the areas presented in red are difficult to achieve with an AM process in general. More precisely, a part requiring high structural integrity is not easy to produce using AM at the present time. A simple solution to increase in the scale is to increase the working environment or to operate many machines in parallel. However, the integrity requires the AM fabrication to make a product with the material whose strength is comparable to the material produced in traditional manufacturing processes. This is the major challenge within the AM community.
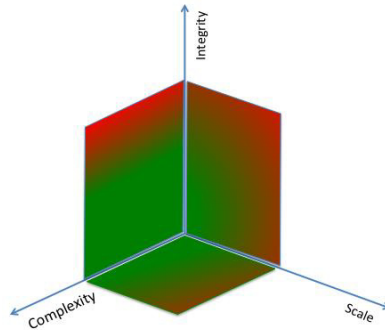

Figure 1: The Current Status of AM Processes among Manufacturing Processes

Because this paper will deals the integrity of the part produced by powder-based AM machine, we will examine the type of the AM technique and the advantage of the particular system we address here. Many types of powder-based AM systems are currently available. Such systems include, 3D printing (3DP), selective laser sintering (SLS), selective laser melting (SLM) and electron beam melting (EBM). These powder-based systems can be distinguished based on two consolidation methods: local and uniform heating. Immediately, the local heating methods such as SLS, SLM and EBM are the main source of inhomogeneity in AM parts. These methods may typically achieve a much higher final density (although not reaching a theoretical density completely) because the material is melted and consolidated with a heating source such as laser or electron beam. Then, during the printing process, the consolidated material below is altered while the material above is consolidating. Therefore, the microstructure is extremely non-uniform and sometimes the residual stresses can be too intense to form cracks in the processed material. This problem can be mitigated by raising the temperature during printing or heat-treating and/or hot-isostatic pressing (HIPing) afterwards to minimize these detrimental defects as well as voids. 3DP is one of the few methods where a part can undergo uniform heating, resulting in a more uniform final microstructure. However, the primary drawback of 3DP is achieving the high relative density, thus the final material properties.

In most processes, the relative density of metallic green parts obtained by 3DP can reach about the 50-60% of a theoretical density. This result is much lower than the green compacts made via powder metallurgy (P/M), which enables up to the 85% of a theoretical density (Allen and Sachs 2000, Farid et al. 2008). In general, the density of a part made from 3DP is much lower than that made form P/M technique. Thus, a post-processing step is necessary to improve the final density of a 3D printed part. After 3D printing, a part is typically infiltrated with a low melting metallic material such as bronze (Allen and Sachs 2000), which change the nature of the material while slightly improves the mechanical properties such as elastic modulus, yield strength, hardness etc. by filling in the pores of the printed material. Few other techniques for making high-dense homogeneous 3DP parts have been published. One of them was the method of infiltrating transient liquid phase that combines through diffusion with the skeletal material to form a desirable final composition (Lorenz et al. 2004). The disadvantage of this infiltration method is that in increases the cost of the entire process. Kakisawa et al. (2005) used fine carbonyl nickel powder (size 5μm) to print parts, and then sinter the parts in order to reach 92% relative density.

The static properties such as hardness, yield strength and elastic modulus of an AM part must reach those of a traditionally processed part if they are expected to use in real applications. Moreover, an AM part is noticeably lacking in its fatigue properties. Instead of the costly measurement of the physical properties of the materials after AM, this paper examines the density of the sintered samples. To make these samples, SS420 powder was mixed with various compounds as possible sintering aids to improving the final density, which is the first step toward improving the integrity of 3DP parts. This approach will lead us to make functional parts, also known as 'direct digital manufacturing' using the powder-based system. One of few machines available in the current market that provide a uniform consolidation condition is 3DP units manufactured by ExOne (N. Huntingdon, PA). This system contains two powder beds: supply and print. The part building process for this device is based on depositing layer by layer of powder while injecting a binder phase at the data points from the given STL file. The required STL file can be created from the simple conversion of a CAD part file.

Our prior research (Sun et al. 2009) demonstrated the effectiveness of ceramic sintering aids for enhancing sintered samples printed from 420 stainless steel. Silicon nitride powder was mixed with stainless steel powder, which enabled us to attain a high relative density (~98%) and excellent mechanical properties (near 200 GPa reported in (Budiniski, K. & Budiniski M. 1999)) sintering at 1300°C with slight distortion on the 3D printed part. However, because of the large amount of silicon nitride (12.5wt% equivalent to 28% volume), the part may not have been considered to be a stainless steel.

In order to reduce the amount of additive utilized, boron based powders including boron (B), boron nitride (BN) and boron carbide (BC) were studied and compared. According to the phase diagram of iron-boron (German and D'Angelo 1984), 1174°C is the liquid-phase formation at eutectic temperature (Figure 1). Its low melting temperature is advantageous because sintering was expecting to take place at a low temperature. In P/M experiments, only 0.4wt% of boron was added to 316 stainless steel and sintered at 1240°C, which enabled them to achieve 99% density (Molinari et al. 1994). This study showed that boron based additives increased the density and decreased the sintering temperature of printed parts significantly.

First, the densification test for many samples at different locations in the powder bed was conducted to test the homogeneity of printed parts. To improve the surface finish, the small particles of additives were aimed at filling in the gaps of the larger particles in order to increase surface quality.
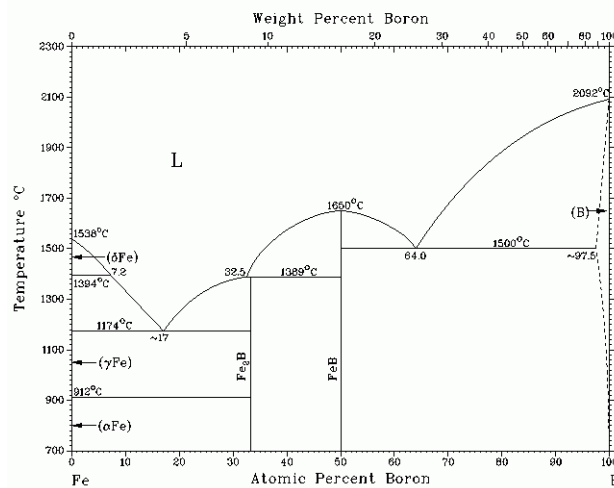

Figure 2: Phase diagram of Iron - Boron

2 Experimental Processing

2.1 Materials and Sample Preparations

The spherical 420 SS powder (Exone, USA) was chosen for this study and it was used in all experiments as the base powder. 420 SS has a particle size distribution range between 22 μm and 53 μm and with a mean size of 30 μm. Three additives, boron (B), boron carbide (BC) and boron nitride (BN), were used as sintering aids, and their material specifications were provided in Table 1.

Table 1: Additives Material Specification

Material	Provider	Average Particle Size μm	Density g/cm^3
B	Sigma Aldrich	1	2.34
BC	Panadyne	0.6	2.51
BN	Sigma Aldrich	1	2.29

For each sintering aid, three experiments were conducted with 0.5 wt%, 1.0 wt% and 1.5 wt% of additive, with one additional comparison sample batch that contains no additives. During each experiment (printing batch), 400 grams of powder mixture was measured and mixed. All powders were measured using Adventurer AR 2140 (Ohaus Corp., Parsippany, NJ, USA) which has a resolution of 0.0001g. A speed mixer DAC 150 (FlackTek, Inc., Landrum, SC, USA) was then used to mix the powder mixture with angular velocity of 2000 rpm and 90 second per cycle for three times. For the density and densification rate experiments, 9 cubic samples were printed with a dimension of 8 mm by 8 mm by 8 mm.

2.2 Materials and Sample Preparations

The printing process involved the use of the X1-Lab 3D printer. This machine operates through the use of two beds: a supply bed and a print bed. Prior to the printing process, the supply bed is lowered as far as it can and filled with the prescribed power mixture (Fig. 2). This ensures that the machine can print as many layers as a design requires. The print bed, however, is raised to the top, so the layers of powder can easily be moved onto it. Once the printing process has begun, a roller moves a layer of power (0.1mm) from the supply bed and layers a layer to the print bed. The machine then lays down a binder phase on top of the layer. Once the next layer is ready to be laid down, the supply bed is raised, so the appropriate amount of powder is exposed, and the print bed is lowered, so the new layer can easily be moved on to it. This process is repeated until the part is completed. In the printing process, the amount of binder phase on each layer has to be controlled such that the layer can bind to the previous layer to form a final shape of a part.

2.3 Density Variation

The deposition variation within the print bed was the first concern. This will result in the size variation depending on the location of a part printed in the powder bed. To study this possibility, nine small cubes were printed and the shrinkage on each cube were measured in a real time while sintering using Thermomechanical Analyzer (TMA) (Setsys Evolution 18 (France)) under the protective environment of argon gas. The final sintering temperature was set at 1400 °C for 6 hours with a temperature rate of 10 °C/min for both heating and cooling cycles, and the final cooling temperature was set at a room temperature.
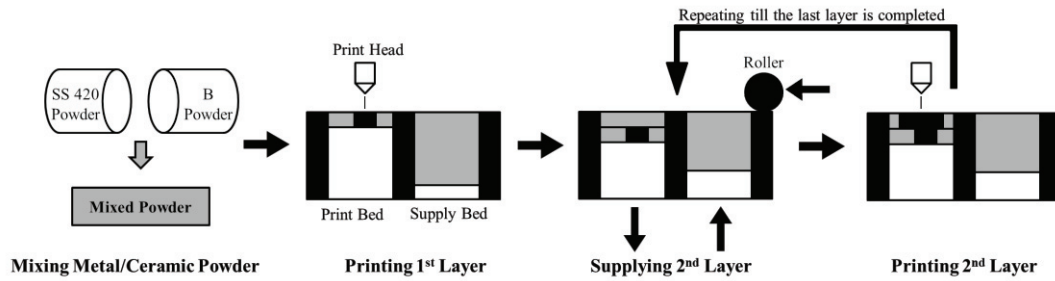
Figure 3: Schematics of 3DP Procedure

2.4 Sintering

The MRF (Materials Research Furnaces) environment-controlled furnace was used to sinter the 3D printed samples. The furnace utilized argon gas to avoid the oxidation. By extracting the gas in the furnace before the sintering begins, the oxidation of the samples was prevented. For the experimental process, the 3D printed samples were separated depending on the sintering temperature. The three temperatures 1150°C, 1200°C, and 1250°C were chosen in this work. In order to reach the sintering temperatures, the samples were places in the furnace and began the heating process starting at room temperature. The furnace then began to heat samples to 240°C at a rate of 10°C/min. Once the furnace reached 240°C, it was kept at this temperature for 2 hour to burn out the binder phase. The binder phase consists of Ethylene Glycol Monobutyl Ether, Ethylene Glycol and Isopropanol which are expected to burn out at the temperatures of 170°C, 197.3°C and 82.6°C, respectively. Thus, at 240°C, these binder phase is completely burned out. Then, the furnace was heated to each prescribed sintering temperature from 240°C at a rate of 5°C/min. Once the samples reached their prescribed sintering temperature, they were kept at this temperature for 6 hours to complete the sintering process of the samples. The samples were then cooled back down to room temperature at a rate of 10°C/min. In order to calculate the relative density, the volume of each fully sintered piece was measured by Archimedes' principle using Adventurer AR 2140 (Ohaus Corp., USA), which has a resolution of 0.0001g.

3 Results and Discussion

3.1 Density Variation

Each printed cube was labeled 1~9, as shown in Figure 3 viewing from the top. During printing, the overall layout was centered to the print bed and each part was spaced evenly; thus it was assumed that cube 5 was the origin, (0,0). All other cubes were either 1 unit away in horizontal direction or vertical direction or both, and their coordinates were assigned accordingly (ex. cube 1 was (-1,1)). After the printing process, the printed samples are very close in the printed dimensions. In order to see the density variation among these samples, the samples were sintered at 1400°C in our TMA.

All samples had similar densification profiles as shown in Figure 4. This is the densification of the cube 1. Each profile was separated into two zones: zone 1 (heating and holding) and zone 2 (cooling). Figure 4 included both temperature (red line) and densification (green line) profiles during the time span. The shrinkage starts at 1200°C and the shrinkage rate increases much faster when the temperature reaches 1400°C. The samples continue to shrink in cooling process so we may increase the density of the final sample by increasing the soaking time (6 hours).
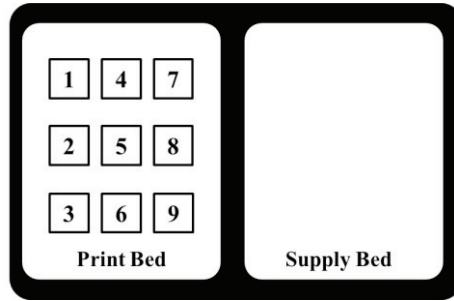
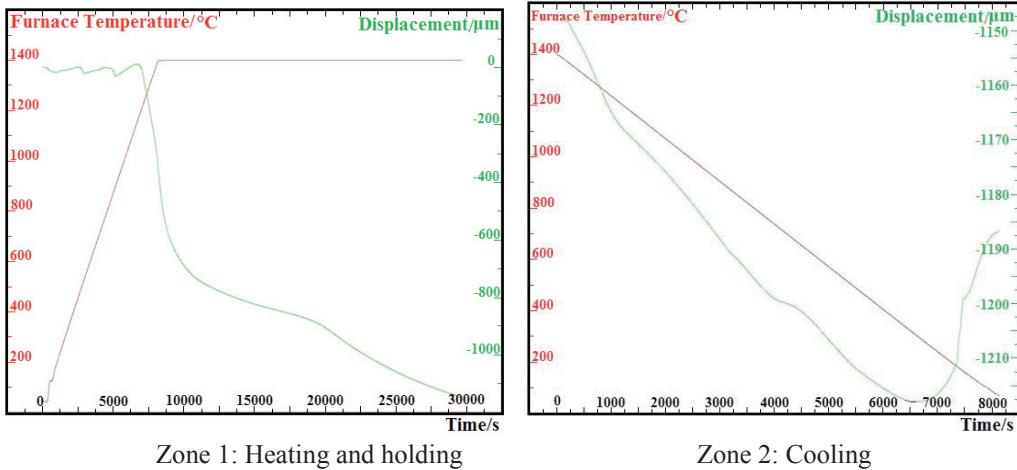Figure 4: Top view of Printed Parts Layout for Each Batch

Zone 1: Heating and holding   Zone 2: Cooling
Figure 5: Densification (Green) and Temperature (Red) Profile for cube 1

A correlation matrix (ranging form -1 to 1) was computed and shown in Table 2 to analyze the relationship between the printed location of each cube and the correlation in shrinkage, both maximum shrinkage and shrinkage at 1400 °C. Shrinkage was converted to positive value prior to the analysis. A significant negative correlation between the shrinkage and horizontal direction indicated that shrinkage increases as the location of cube moves to the left (negative direction); and near to zero correlation between the shrinkage and vertical direction implied that vertical location was not a significant factor for shrinkage. As the roller spread the power from the right side of power bed to the left side, the right side of the powder bed had a higher compact factor since more powder exists at the beginning (the right side) on each layer than at the end (the left side). Therefore, the parts printed on the left side of the powder bed would experience more shrinkage as observed during TMA experiment.

Table 2 Correlation Matrix of Shrinkage in Horizontal & Vertical Directions

	Correlation in Maximum Shrinkage	Correlation in Shrinkage at 1400 °C
Horizontal Direction	-0.8205	-0.71688
Vertical Direction	0.052274	0.133584

3.2   Liquid Phase Sintering

Ea sample was polished using diamond polishing solution with the grit size of 1 μm for 30 minutes and etched with the solution made of 10 mL HNO_3, 20mL HCl and 30 mL water for a few seconds. Then it was examined under optical microscope to visualize the microstructure. Figure 5(a, b, c) shows the microstructures of the samples with 0.5% of B additives sintered at 1150°C, 1200°C and 1250°C, respectively. Figure 5(b) shows that the samples sintered at 1200°C had liquid phase present as powders started to group themselves compared to Figure 5(a) where the powders in their original spherical shapes remained the same. Figure 5(c) shows the formation of much larger grains and grain boundaries. It indicates that the grains have coalesced into larger grains. Figure 5(c) also shows necklace microstructure between grains, indication of liquid phase sintering (Riegger, Pask and Exner 1980, Warren and Waldron 1972). Similar microstructure behavior can be observed in the samples with the other two additives sintered at higher temperature, liquid phase sintering started to occur based on the presence of the necklace microstructure.
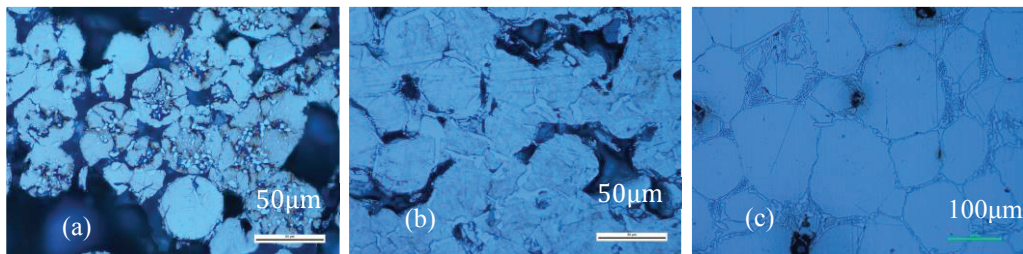

(a) 0.5% B sintered at 1150°C   (b) 0.5% B sintered at 1200°C   (c) 0.5% B sintered at 1250°C

Figure 6: Microstructures of the Selected Sintered Samples.

3.3   Surface Quality

One of the important issues with 3D printing is the surface quality. Because of its characteristic building process, the layering is evident on the side surfaces of the printed part. It improves little after sintering. Using the bimodal-sized powder, Lanzetta and Sachs (2003) increase not only the density of the sample (because the multiple powder sizes can increase the packing density) but also the surface quality of the samples. However, sometime the mixing two diistinct powders is difficult. The slurry method (Moon et al. 2000) is used with the bimodal powder because small particles are difficult to be spread when they are dry and the amount of fine powder is more than 25%wt. However, this study used only small amounts of fine additive powder and the high speed mixing process described in Section 2.1 was very effective.

The surface roughness of each sample after sintering is measured by a Zeiss LSM 210 Confocal Laser Scanning Microscope. Figure 6 shows the topography of three sintered samples at 1250°C with 0.5% boron carbide, 0.5% BN and pure stainless steel. The surface roughness decreases significantly in the samples with the additives. Especially, the sample with 0.5% BC sintered at 1250°C formed liquid phase and provide the smooth surface. The average roughness value, R_a, improve from 9.01 μm with pure stainless steel to 8.2 μm with 0.5% BN and 6.22 μm with 0.5% BC.
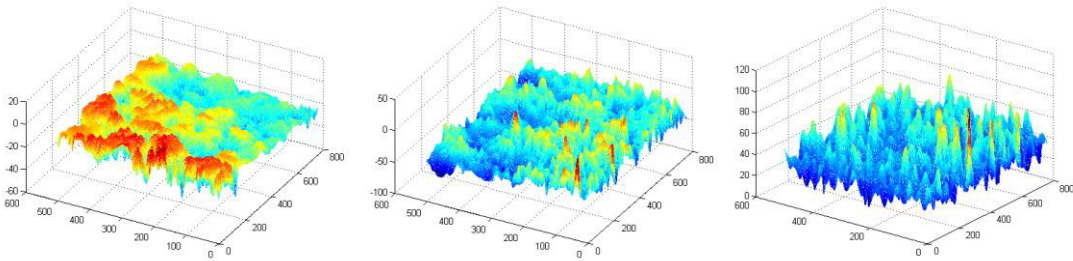
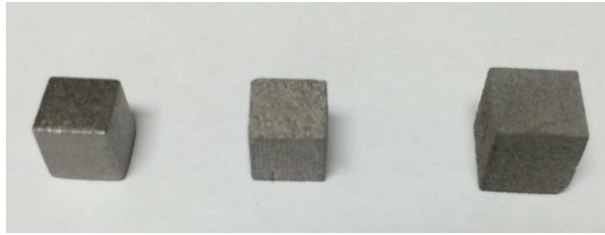(a) BC   (b) BN   (c) Pure Stainless Steel

Figure 7: Topography of the Samples sintered at 1250C with 0.5 % wt additive of (a) BC, (b) BN and (c) Pure Stainless Steel.

3.4 Densification

The SS420 powder samples were mixed with the 0.5%, 1% and 1.5% wt of the three additives, B, BN and BC. Each of these samples was sintered at the temperatures of 1150°C, 1200°C and 1250°C. The density of each sample after sintering was measured using the Archimedes principal. As shown in Table 3, the additives did not necessary increase the density of the samples after sintering at 1150°C. Raising the sintering temperature from 1150°C to 1200°C and 1250°C has increased the densities in each case. For each sintering temperature, it was found that the samples with 1% wt B additives had the highest densities. Among the samples with BN additives, the samples with 1% wt BN additive had the highest densities. The highest relative density was attained with the sample with 1% wt B additive at approximately 97%. There was a dramatic drop in the relative density from the 1% wt of B to the 1.5% wt of B at 1250°C because the latter sample formed extensive liquid phase during sintering. With the presence of the extensive liquid phase, pores were generated, which were also observed in (Moon et al. 2000). The liquid phase caused the distortion in the samples with 1.0% wt B and BC additives at both 1200°C and 1250°C and the sample with 1.0% wt BN additives at 1250°C. The samples with 1.5% wt of all additives sintered at 1250° have distorted the shape extensively. The distortion is based on the observation of the shape of the cubic samples as presented in Figures 7 and 8. The sample with 0.5% wt of B additive sintered at 1250° was also distorted. The sample with 0.5% wt of BN and BC sintered at 1250°C remained the same shape as shown in Figure 7 (a and b). The sample with the highest density that maintains its shape was the 0.5% BC sample sintered at 1250°C with a relative density of 90.22%.

Table 3: The Final Relative Densities After Sintering with and without the additives

Relative Density	Boron			Boron Nitride			Boron Carbide			No additive
Sintered at	0.5%	1.0%	1.5%	0.5%	1.0%	1.5%	0.5%	1.0%	1.5%	
1150 °C	52.95%	55.33%	54.56%	51.80%	53.58%	49.74%	53.35%	53.33%	50.24%	55.32%
1200 °C	77.82%	83.02%	68.34%	59.31%	77.72%	56.10%	75.80%	74.83%	65.79%	63.16%
1250 °C	90.70%	96.98%	80.57%	87.62%	91.41%	90.18%	90.22%	93.97%	83.46%	64.58%

(a) 0.5% wt BC (b) 0.5% wt BN   (c) Pure Stainless Steel
Figure 8: The Undistorted Samples After Sintering at 1250°C

(a) 1.5% wt B (b) 1.5% wt BN   (c) 1.5% wt BC
Figure 9: The Distorted Samples After Sintering at 1250°C

4   Conclusions

The 3D printing and sintering process were used to make parts from SS420 stainless steel powder with boron-based additives. The effect of additive contents and sintering temperature are studied on the relative densities of the final parts.

(1) A slightly variation in the densification rate of samples depending on the locations in the print bed. It can be explained by the variation in the powder packing as the roller moves from the right to the left. More powder is present at the right side of the print bed during the powder spreading.

(2) The powder samples mixed with the smaller additives help to improve the final surface finish substantially. Not only the smaller additives fill into the interstitial spaces among large particles but also the additives enhance diffusion among the stainless steels powder.

(3) The highest dense obtained is 97% with the sample containing 1% B and sintered at 1250°C. However, the sample was extensively distorted because of the extensive formation of liquid phase.

(4) The densest sample that maintained the original shape without distortion was the 0.5% wt BC sintered at 1250°C at the relative density of 90.22%. Based on the result, the future work will concentrate on fine-tuning the amount of additive around 0.5% and sintering temperature 1250°C.

(5) The extensive distortion is evident with B additive. By reducing the sintering temperature, the use of B may improve the final shape.

References

Allen, SM & Sachs, EM 2000, 'Three-Dimensional Printing of Metal Parts for Tooling and Other Applications,' *Met. Mater. (Seoul, Rep. Korea)*, vol. 6, no. 6, pp. 589–594.

Budinski, KG & Budinski, MK 1999, *Engineering Materials: Properties and Selection*, 6th edn., Prentice-Hall, Englewood Cliffs, NJ.

Conner, BP, Manogharan, GP, Martoff, AN, Rodomsky, LM, Rodomsky, CM, Jordan, DC & Limperos, JW 2014, 'Making Sense of 3-D Printing: Creating a map of Additive manufacturing Products and Services,' *Additive Manufacturing*, vol. 1-4, October, pp. 64-76

Farid, A, Feng, P, Du, X, Jawid, A., Tian, J & Guo, S 2008, 'Microstructure and Property Evolution During the Sintering of Stainless Steel Alloy With Si3N4,' *J. Mater. Sci. Eng.*, vol. 472, pp. 324–331.

German, RM & D'Angelo, KA 1984, 'Enhanced Sintering treatments for Ferrous Powder,' *International Metals Reviews*, vol. 29, no. 1, pp. 249-272.

Kakisaw, H, Minagawa, K, Ida, K, Maekawa, K & Halada, K 2005, 'Dense O.M Component Produced by Solid Freefrom Fabrication (SFF),' *Materials Transactions*, vol. 46, no. 12, pp. 2574-2581.

Lanzetta, M & Sachs, E 2003, 'Improved surface finish in 3D printing using bimodal powder distribution,' *Rapid Prototyping Journal*, vol. 9, no. 3, pp. 157-166.

Lorenz, A, Sashs, E, Allen, S, Rafflenbeul, L & Kernan, B 2004, 'Densification of a Powder-Metal Skeleton by Transient Liquid-Phase Infiltration,' *Metall. Mater. Trans. A*, vol. 35A, pp. 631–640.

Molinari, A, Kazior, L, Marchetti, F, Canteri, R, Cristofolini I & Tiziani A 1994, 'Sintering mechanisms of boron alloyed AISI 316 stainless steel,' *Powder Metallurgy*, vol. 37, no. 2, pp. 115-112.

Moon, J, Grau, JE, Cima, MJ & Sachs, EM 2000, 'Slurry chemistry control to produce easily redispersible ceramic powder compacts,' *Journal of the American Ceramic Society*, vol. 83, no. 10, pp. 2401-3.

Riegger, H, Pask, JA & Exner, HE 1980, *In: Kuczynski GC (ed) Sintering processes*, Plenum Press, New York, pp 219-233.

Sun, L., Kim, YH, Kim, D & Kwon, P 2009, 'Densification and Properties of 420 Stainless Steel Produced by Three-Dimensional Printing with Addition of Si3N4 Powder,' *Journal of Manufacturing Science and Engineering*, vol. 131, no. 6, doi:10.1115/1.4000335.

Warren, R & Waldron, MB 1972, 'Microstructural development during the liquid phase sintering of cemented carbides,' *Powder Metall*, vol. 15, pp. 166-201.